



UNIVERSITÀ
DEGLI STUDI
FIRENZE

FLORE

Repository istituzionale dell'Università degli Studi di Firenze

Functionalised Nanoclays as Microstructure Modifiers for Calcium and Magnesium Silicate Hydrates

Questa è la Versione finale referata (Post print/Accepted manuscript) della seguente pubblicazione:

Original Citation:

Functionalised Nanoclays as Microstructure Modifiers for Calcium and Magnesium Silicate Hydrates / Ferraro, Giovanni; Romei, Lisa; Fratini, Emiliano; Chen, Sow-Hsin; Jeng, U-Ser; Baglioni, Piero. - In: PHYSICAL CHEMISTRY CHEMICAL PHYSICS. - ISSN 1463-9076. - STAMPA. - (2021), pp. 0-0. [10.1039/D0CP06251K]

Availability:

The webpage <https://hdl.handle.net/2158/1221386> of the repository was last updated on 2021-01-14T09:21:55Z

Published version:

DOI: 10.1039/D0CP06251K

Terms of use:

Open Access

La pubblicazione è resa disponibile sotto le norme e i termini della licenza di deposito, secondo quanto stabilito dalla Policy per l'accesso aperto dell'Università degli Studi di Firenze (<https://www.sba.unifi.it/upload/policy-oa-2016-1.pdf>)

Publisher copyright claim:

La data sopra indicata si riferisce all'ultimo aggiornamento della scheda del Repository FloRe - The above-mentioned date refers to the last update of the record in the Institutional Repository FloRe

(Article begins on next page)

PCCP

Physical Chemistry Chemical Physics

Accepted Manuscript

This article can be cited before page numbers have been issued, to do this please use: G. Ferraro, L. Romei, E. Fratini, S. Chen, U. Jeng and P. Baglioni, *Phys. Chem. Chem. Phys.*, 2021, DOI: 10.1039/D0CP06251K.



This is an Accepted Manuscript, which has been through the Royal Society of Chemistry peer review process and has been accepted for publication.

Accepted Manuscripts are published online shortly after acceptance, before technical editing, formatting and proof reading. Using this free service, authors can make their results available to the community, in citable form, before we publish the edited article. We will replace this Accepted Manuscript with the edited and formatted Advance Article as soon as it is available.

You can find more information about Accepted Manuscripts in the [Information for Authors](#).

Please note that technical editing may introduce minor changes to the text and/or graphics, which may alter content. The journal's standard [Terms & Conditions](#) and the [Ethical guidelines](#) still apply. In no event shall the Royal Society of Chemistry be held responsible for any errors or omissions in this Accepted Manuscript or any consequences arising from the use of any information it contains.

ARTICLE

Functionalised Nanoclays as Microstructure Modifiers for Calcium and Magnesium Silicate Hydrates†

Giovanni Ferraro^{a,§}, Lisa Romei^{a,§}, Emiliano Frattini^{a,*}, Sow-Hsin Chen^b, U-Ser Jeng^c, Piero Baglioni^aReceived 00th January 20xx,
Accepted 00th January 20xx

DOI: 10.1039/x0xx00000x

Calcium silicate hydrate (C-S-H) is the main binding product of ordinary Portland concrete (OPC). Unfortunately, OPC production generates ~5% of all anthropomorphic CO₂. Among the most promising green alternatives, magnesium silicate hydrate (M-S-H) is a colloidal gel equivalent to C-S-H which exhibits weaker mechanical properties. Here we investigated the effect of the inclusion of aluminosilicate nanoclays (HNTs) on the microstructure of the silicate hydrate gels as a strategy to ultimately improve their mechanical properties. The microstructure of C-S-H and M-S-H gels synthesized with and without carboxylic or polycarboxylic functionalised HNTs (HNT-COOH, HNT-PAA) has been investigated by a multi-technique approach including small- and wide-angle X-ray scattering (SWAXS) and scanning electron microscopy (SEM). The results indicate that, during C-S-H formation in solution, HNTs decrease the size of the disk-like globules with little influence on the spacing of calcium silicate layers. In the case of M-S-H, the presence of functionalised HNTs has a reduced effect on the hydrate structure as a result of the weaker interaction of the carboxylic moieties with Mg²⁺ ions. SEM investigation on the synthesized composites shows that HNT-PAA are better included in the hydration products. Moreover, in the proximity of the PAA functionalised surfaces less extended aggregates are formed while the micron size morphology of both M-S-H and C-S-H with HNT-COOH is conserved.

Introduction

An important issue with commonly used ordinary Portland cement (OPC) is that its production process generates an enormous amount of carbon dioxide¹. Therefore, for a sustainable construction policy, it is crucial to reduce OPC carbon footprint or focus on alternatives generating less CO₂. Magnesium-based “green” cement is one of the several possible alternatives to partially or entirely substitute OPC². According to previous studies³, highly reactive MgO can be obtained starting from magnesium silicates. Unfortunately, the mechanical properties of “green” magnesium-based cement, especially the compressive strength, are not as high as for OPC⁴. Nevertheless, it is possible to improve the mechanical properties of “green” cement, for example, by adding reinforcement additives. Recent studies demonstrated that the addition of a small amount of additives can deeply change the properties of cement mortars and concretes^{5,6}. Among various class of additives, halloysite nanoclays have gained increasing attention in the last years due to their availability, low cost, and an increase of the mechanical properties of the final

composite^{5,6}. In particular, it was proven that the incorporation of 3% nanoclays in mortars improves the compressive strength by up to 24%⁷. These additives act as fillers thanks to their nanosized dimension while the tubular shape favours their capacity to crosslink the cement matrix. Allalou *et al.*⁸ demonstrated that the addition of halloysite nanoclays in cement pastes can improve the early age and long-term mechanical strength due to the formation of additional hydrated products during the curing process. Similar results were observed by Hosseini *et al.*⁹, where it has been proven that nanoclays can improve the microstructure of cement mortar and, consequently, develop additional mechanical strength and durability. In particular, they observed that the inclusion of about 20% of nanoclay/aminosilane mixture introduces a microstructural regularity in cement mortars. A recent study reports the use of halloysites as nano-carriers of corrosion inhibitors in cement formulations¹⁰. In particular, the active molecule released from the nanoclays can migrate in the water to reach the internal matrix thus preventing the corrosion degradation. Despite the large number of publications on the effect of these additives on the hydration and mechanical properties of the cement mortars, an in-depth investigation on the effect of halloysites on the developing microstructure of the silicate hydrate phases is still missing. In addition, to the best of our knowledge, there are no studies dealing with the structural effect of these nanoclays on magnesium-based cement. To fill this gap, this study reports the investigation of the microstructure of calcium and magnesium-based composites with nanoclays. In particular, nanoclays (HNTs) functionalised with carboxylic or polycarboxylic groups (HNT-COOH and HNT-

^a Department of Chemistry “Ugo Schiff” & Consorzio per lo Sviluppo dei Sistemi a Grande Interfase (CSGI), University of Florence, Via della Lastruccia, 3, 50019 Sesto Fiorentino, Italy.

^b Department of Nuclear Science and Engineering, Massachusetts Institute of Technology, Cambridge, Massachusetts 02139, USA

^c National Synchrotron Radiation Research Center, Hsinchu Science Park, Hsinchu 30076, Taiwan.

Email address: emiliano.frattini@unifi.it.

§ These authors contributed equally to this work.

† Electronic Supplementary Information (ESI) available. See DOI: 10.1039/x0xx00000x

ARTICLE

PCCP

PAA, respectively) have been used to modify the microstructure of C-S-H and M-S-H pure phases while developing in solution. Their influence on the microstructure of the gels has been investigated by a multi-technique approach including small- and wide-angle X-ray scattering (SWAXS) and scanning electron microscopy (SEM). SAXS curves were analysed using the models proposed in a previous work by some of the authors¹¹. In particular, C-S-H gels were modelled considering that they are formed by discoidal globules which pack into a mass fractal structure. The globule contains alternating C-S-H and water layers with a thickness of several angstroms. This lamellar arrangement results in a small peak⁵ in the C-S-H SAXS pattern at about 0.5 \AA^{-1} . On the contrary, M-S-H samples were considered as composed by a fractal structure of polydisperse spheres. The addition of the HNTs, especially if functionalised by PAA, causes remarkable changes in the microstructure of the C-S-H phases, while less significant modifications are observed for M-S-H probably as a consequence of the diverse chemical interaction of the carboxylic moieties with the Ca^{2+} and Mg^{2+} ions.

Experimental details

Materials

Sodium metasilicate pentahydrate ($\text{Na}_2\text{SiO}_3 \cdot 5\text{H}_2\text{O}$, >95%, Sigma-Aldrich), calcium nitrate tetrahydrate ($\text{Ca}(\text{NO}_3)_2 \cdot 4\text{H}_2\text{O}$, >99%, Sigma-Aldrich), magnesium nitrate hexahydrate ($\text{Mg}(\text{NO}_3)_2 \cdot 6\text{H}_2\text{O}$, 99%, Sigma-Aldrich), halloysite nanoclays (HNT, $\text{Al}_2\text{Si}_2\text{O}_5(\text{OH})_4 \cdot 2\text{H}_2\text{O}$, Sigma-Aldrich), (3-aminopropyl)triethoxysilane (APTES, $\text{H}_2\text{N}(\text{CH}_2)_3\text{Si}(\text{OC}_2\text{H}_5)_3$, 99%, Sigma-Aldrich), succinic anhydride ($\text{C}_4\text{H}_4\text{O}_3$, >99%, Sigma-Aldrich), 3-(Trimethoxysilyl)propyl methacrylate (TMSPMA, $\text{H}_2\text{C}=\text{C}(\text{CH}_3)\text{CO}_2(\text{CH}_2)_3\text{Si}(\text{OCH}_3)_3$, 98%, Sigma-Aldrich), acrylic acid (AA, $\text{CH}_2=\text{CHCOOH}$, 99%, Sigma-Aldrich), Ammonium persulfate ($(\text{NH}_4)_2\text{S}_2\text{O}_8$, 99%, Sigma-Aldrich), ethanol ($\text{CH}_3\text{CH}_2\text{OH}$, >99.8%, Sigma-Aldrich), ammonium hydroxide solution (28% NH_3 in H_2O , Sigma-Aldrich). All chemicals were used as received. Milli-Q water (18.2 M Ω) was used for all the experiments.

Samples preparation

The pure silicate hydrate phases of magnesium (M-S-H) and calcium (C-S-H) were prepared through a double-decomposition synthesis following the procedure described by Brew and Glasser¹². Briefly, stock solutions of calcium nitrate, $\text{Ca}(\text{NO}_3)_2 \cdot 4\text{H}_2\text{O}$, or magnesium nitrate, $\text{Mg}(\text{NO}_3)_2 \cdot 6\text{H}_2\text{O}$, were slowly added to sodium metasilicate, $\text{Na}_2\text{SiO}_3 \cdot 5\text{H}_2\text{O}$, solution under stirring in a two-necked round-bottomed flask under continuous N_2 flux while cooled in an ice bath. The Ca/Si and Mg/Si ratios were chosen equal to 1. The precipitate was washed under a N_2 atmosphere (to avoid carbonation) with milli-Q water to remove unreacted counter ions. Analogous samples containing HNT properly functionalised with carboxylic or polycarboxylic groups (HNT-COOH, HNT-PAA) were also prepared with a nanoclays/M molar ratio of 0.08 (where M=Mg, Ca). The details on the HNT functionalization with carboxylic¹³ (-COOH) or polycarboxylic¹⁴ (-PAA) groups are reported in the ESI

file. The samples were investigated after controlled dehydration at 60 °C in order to obtain a water/solid ratio of about 0.3 to mimic the water content usually present in a cement paste. Such mild temperature was chosen to gently evaporate water without causing structural damages to the gel phase.

Small- and wide-angle X-ray scattering (SWAXS)

SWAXS measurements were performed at the National Synchrotron Radiation Research Center (NSRRC), (Hsinchu, Taiwan) using the BL23A beamline¹⁵. The sample-to-detector distance was set 1.33 m for WAXS (detector C9728DK) and 4.95 m for SAXS (Pilatus 1 MF detector). The scattering vector, Q , was calibrated using silver behenate for SAXS and sodalite and silicon powders for WAXS. The Q range investigated for WAXS was $0.5 - 5.5\text{ \AA}^{-1}$ and $0.002 - 0.55\text{ \AA}^{-1}$ in the case of SAXS experiments. Samples were sealed in 1 mm cells (X-ray path length) and measured at room temperature. The electronic noise, sample transmission, background scattering and detector sensitivity were subtracted from the obtained data and the curves were scaled to absolute intensity using the scattering of a standard sample of high-density polyethylene using procedure developed at NSRRC. The analytical models for the analysis of the SAXS curves of the pure phases are detailed in the ESI file.

Field emission scanning electron microscopy (FE-SEM)

Field Emission Scanning Electron Microscopy (FE-SEM) was performed with a SIGMA high-resolution scanning electron microscope (Carl Zeiss Microscopy GmbH, Germany). All the micrographs were acquired on the uncoated samples after lyophilization, using an acceleration potential of 5 kV and a working distance of about 3 mm.

Infrared spectroscopy (IR)

Infrared spectroscopy was performed by a Nexus 870 FT-IR spectrometer from Thermo Nicolet. Data were collected at room temperature in attenuated total reflectance (ATR) mode. The optical resolution was 4 cm^{-1} and the investigated spectral range was from 400 to 4000 cm^{-1} . A total of 128 scans were gathered for each sample to get an acceptable signal-to-noise ratio.

Results and discussion

Morphology and nanostructure of the pure silicate phases (C-S-H and M-S-H) have been already investigated and fully discussed in a previous work by some of the authors¹¹. Briefly, the M-S-H gel (see Figure S5 in ESI file) shows the presence of spherical particles with dimensions around 10 nm characterized by a high polydispersity, while the C-S-H sample (see Figure S6 in ESI file) exhibits a foil-like structure.

Halloysite nanoclays are characterized by a tubular shape with different length (from 100 nm to 10 μm) and a wall thickness of about 20-30 nm with a cavity ranging from 40 to 60 nm (see Figure S7 in ESI file). The comparison of pure halloysites (HNT) and halloysites functionalised with carboxylic and polycarboxylic groups (HNT-COOH and HNT-PAA, respectively)

reveals no evident morphological differences associated to the functionalization procedure. HNT-PAA show a structural organization in globules and are less stable under the electron beam during SEM analysis, probably as a result of the presence of a larger organic shell on the external surface with respect to the other nanoclays.

SEM micrographs of the composite samples C-S-H and M-S-H with HNT-COOH and HNT-PAA at two different magnifications are reported in Figure 1.

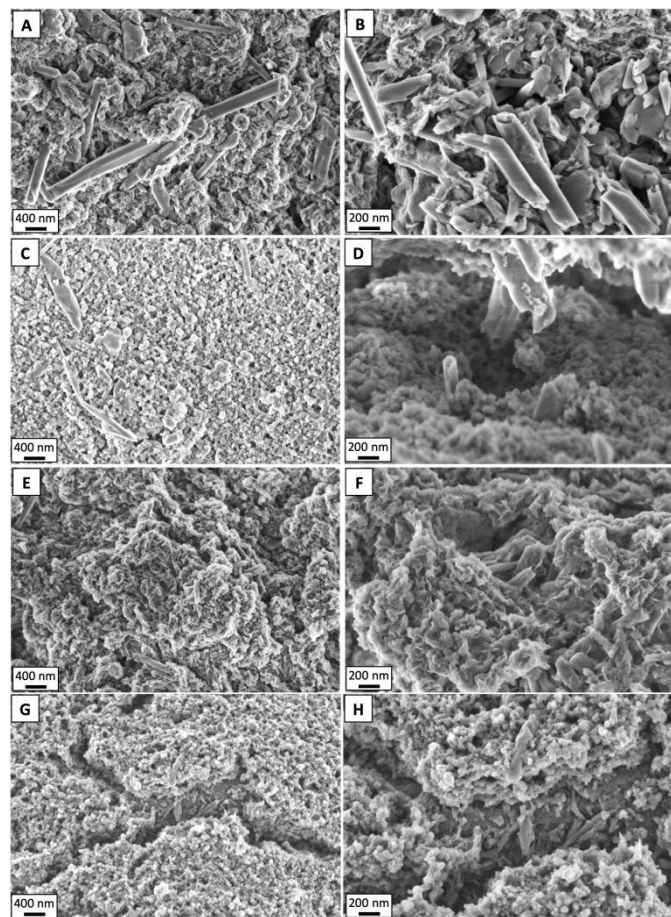


Fig. 1 SEM micrographs of all the investigated samples at two different magnifications (50 kX left, 100 kX right): C-S-H@HNT-COOH (panels A-B), M-S-H@HNT-COOH (panels C-D), C-S-H@HNT-PAA (panels E-F) and M-S-H@HNT-PAA (panels G-H).

The morphology of the silicate hydrate phases in the composite samples at the micrometric level is partially affected by the presence of the HNTs additives. In particular, the halloysites are well distributed in the samples both on the surface and inside the matrices. This result shows a good chemical compatibility of the developing silicate hydrates with the nanoclays functionalised by COOH moieties or PAA chains.

HNT-PAA nanoclays in the composites (Figure 1, panels E-H) appear to be more incorporated in the silicate matrices with respect to HNT-COOH (Figure 1, panels A-D) and their surface completely covered by the hydration products. Moreover, in the presence of HNT-PAA it is clear that the formation of the extended typical C-S-H laminar pattern is inhibited with the arrangement of the gel in less extended foils. Structural changes

induced by polycarboxylates-based super-plasticizers have been recently observed through small-angle neutron and X-ray scattering studies showing that these additives enhance the formation of foil-like morphologies in the C-S-H gel.¹⁶

The structure of the different phases at the atomic level can be evaluated from wide-angle X-ray scattering (WAXS). Figure 2 reports the WAXS curves of pure phases and the same phases growth in the presence of functionalised HNTs: HNT-COOH, HNT-PAA, M-S-H, M-S-H@HNT-COOH, M-S-H@HNT-PAA, C-S-H, C-S-H@HNT-COOH and C-S-H@HNT-PAA.

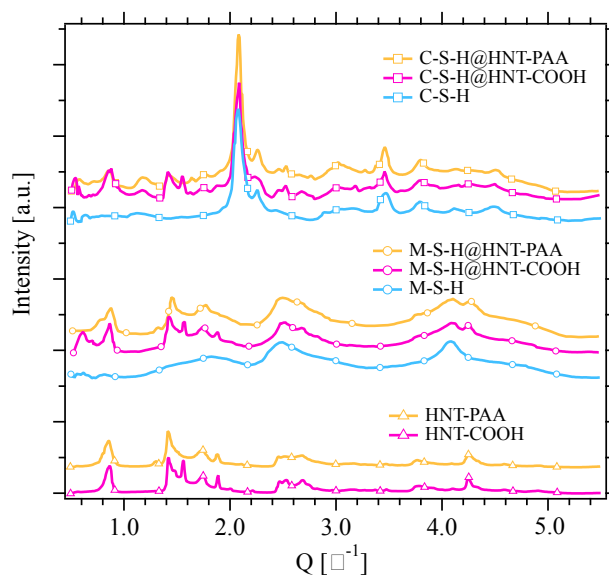


Fig. 2 WAXS curves for: M-S-H@HNT-COOH, M-S-H@HNT-PAA, C-S-H@HNT-COOH and C-S-H@HNT-PAA. WAXS patterns for the pure hydrates (C-S-H, M-S-H), and HNT additives (HNT-COOH, HNT-PAA) are reported as a comparison.

The signals in the HNT-COOH and HNT-PAA patterns are the reflections due to the spacing between the aluminum-silicates sheets constituting the walls of the nanotube (see ref.¹⁷ and references therein). In particular, the peak centred at 0.8 \AA^{-1} corresponds to the multilayer wall packing characteristic of the nanoclays, while the peaks centred at 1.4 and 1.5 \AA^{-1} indicate the presence of a kaolin-type mineral. The diffractogram of the pure M-S-H shows the characteristic peaks of Magnesite (MgCO_3) and Lizardite ($\text{Mg}_3\text{SiO}_5(\text{OH})_4$)^{18,19}. The absence of the characteristic peaks related to Brucite ($\text{Mg}(\text{OH})_2$) can be justified considering that in our experimental conditions the amount of precipitated $\text{Mg}(\text{OH})_2$ phase is too low to be detected by XRD¹². The broadening of the peaks evidences the gel-like nature of this phase. In the case of C-S-H sample, Tobermorite ($\text{Ca}_5(\text{Si}_6\text{O}_{16}(\text{OH})_2)_4 \cdot 4(\text{H}_2\text{O})$) is the main component²⁰ and the presence of sharper peaks with respect to M-S-H evidences a more ordered structure.

In the composite samples, the co-presence of the contributions related to the different pure phases is clearly visible, thus confirming that halloysites do not change the arrangement of the silicate hydrates at the atomic level.

At the nanometric level the structural effect of the HNTs on the hydrate phases was evaluated by means of small angle X-ray

scattering (SAXS). The scattering profiles of pristine and functionalised HNTs, the pure silicate hydrate phases and the corresponding composites are reported in Figure 3.

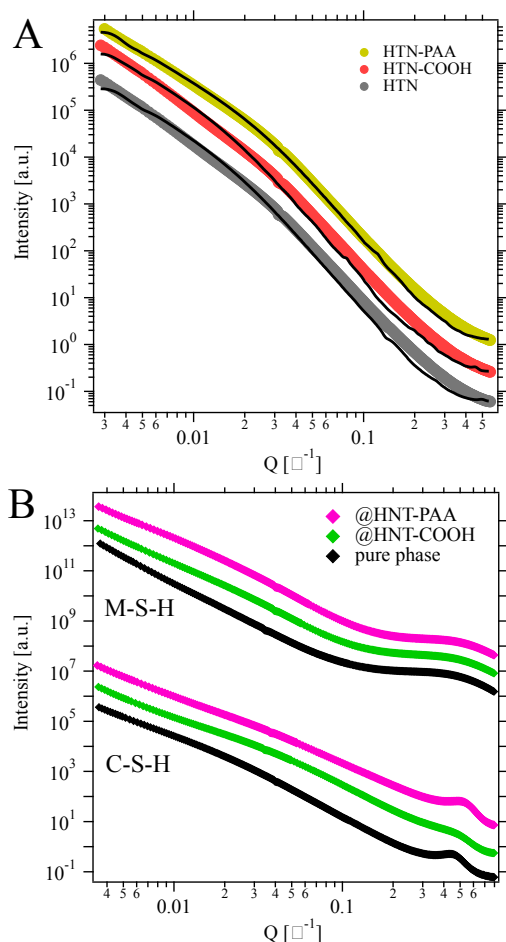


Fig. 3 Panel A: SAXS curves of HNT (grey markers), HNT-COOH (red markers) and HNT-PAA (yellow markers). The experimental points (markers) and associated fits (lines) are shifted along y-axis for clarity. The fitting residuals are reported in ESI file. Panel B: SAXS curves of C-S-H and M-S-H pure phases (black markers) and composites with HNT-COOH (green markers) and HNT-PAA (pink markers).

In the case of nanoclays, the SAXS patterns reported in Figure 3A are analysed using the hollow cylinder model with a polydispersity on the wall thickness and core radius (details on the model are reported in ESI file)²¹. Table 1 lists the parameters obtained from the fitting. The geometrical descriptors obtained from the fitting are in good agreement with the sizes observed from SEM micrographs. These results show that the functionalization of the nanotubes with COOH groups and PAA fragments does not significantly affect the nanostructure of the bare HNTs.

The scattering profiles of the pure phases and relative composites obtained in the presence of the two functionalised HNTs are shown in Figure 3B. The structural information of the silicate phases can be obtained analysing SAXS curves with a multilayer disk-like globular model in the case of C-S-H or a spherical globular model for M-S-H as discussed in our previous works^{11,16}.

Table 1 Parameters obtained by analysing the scattering curves of the different additives (HNT, HNT-COOH and HNT-PAA) with the hollow cylinder model. The radius of the halloysite framework resulted in all cases about $11 \cdot 10^{-6} \text{ Å}^2$. The effect of the functionalization did not change this value being the electron density mainly concentrated on the aluminosilicate matrix. Values in parentheses are standard deviations on the last significant figures. The length of the cylinder is outside the dimensional range explored by the present SAXS experiment. Its value was arbitrary fixed to 2 nm. It is important to note that any variation in the micron range was not affecting the results of the other fitting parameters.

	HNT	HNT-COOH	HNT-PAA
Radius (nm)	203.0 (2)	202.8 (1)	207.4 (1)
polydispersity	0.11 (1)	0.11 (1)	0.12 (1)
Thickness (nm)	8.8 (2)	8.6 (2)	6.2 (3)
polydispersity	0.62 (1)	0.62 (1)	0.66 (1)

However, these models do not take into account the contribution coming from the additives; therefore, the fitting is performed on the curves after the subtraction of additives' contribution assuming that the HNT scattering is unchanged while the additive is in the composite. All the differences found with respect to a simple linear combination of the SAXS patterns coming from the pure phases are allocated to an excess of scattering due to a diverse nucleation and growth induced on the silicate hydrates by the presence of the HNTs. The details about the procedure used to estimate the scattering contribution of the additives in the SAXS patterns obtained from the composites are reported in the ESI file. Figure 4 shows the scattering curves obtained after additives subtraction along with the best fit results. The models used to analyse the curves after the subtraction are discussed in ESI file while all the parameters used for the data fitting are listed in Table 2.

The obtained results show that the effective size of the globules in the two phases decreases in the presence of the additives. Comparing C-S-H (pure phase) with the composites containing HNT-COOH or HNT-PAA, it is evident that the presence of the nanoclays reduces the effective size of the globules (R_e 90.2 Å, 43.4 Å and 45.6 Å, respectively). For these samples, also the average number of layers "n" decreases in the presence of the nanoclays additives. The Schultz distribution of the total thickness "t" of the multilayer disk-like globules in C-S-H samples (see Figure 5A) indicates that the total thickness ($t = nL$) decreases from 46.6 Å for the pure phase to 24.7 Å and 27.2 Å for the composites with HNT-COOH and HNT-PAA, respectively. The standard deviation associated to the total thickness ($\sigma = nL/(Z_n + 1)^{1/2}$) are 27.3 Å, 10.1 Å and 21.8 Å for the pure phase, HNT-COOH and HNT-PAA composites, respectively. The same trend is obtained for M-S-H, in which the size of the globules (R) decreases passing from 19.5 Å (pure phase) to 8.8 Å for both the samples containing HNTs. The deviations associated to the radius distribution $\sigma = R/(Z_R + 1)^{1/2}$ (see Schultz distribution in Figure 5B) is 16.0 Å for the pure phase, 7.4 Å for the composite with HNT-COOH and 7.5 Å for the composite with HNT-PAA. The smaller dimension of the globules obtained in the composites could be ascribed to the presence of the nanoclays, which act as nucleation site favouring the formation of smaller domains during the silicate formation.

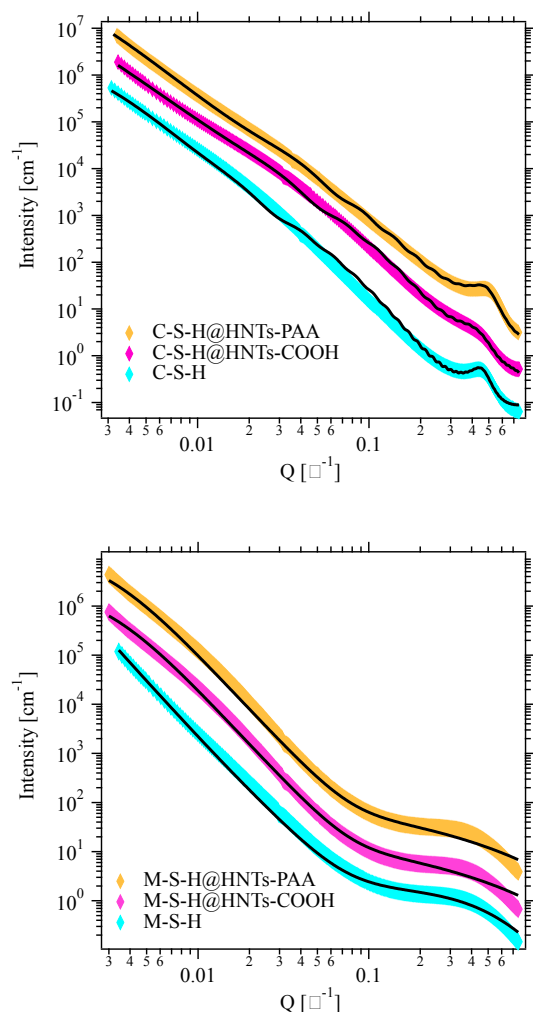


Fig. 4 SAXS curves of the pure phases (light blue markers) and composites containing HNT-COOH (pink markers) and HNT-PAA (orange markers) along with the best fit (black lines). The experimental intensities are shifted along y-axis for the sake of clarity. The fitting residuals are reported in ESI file.

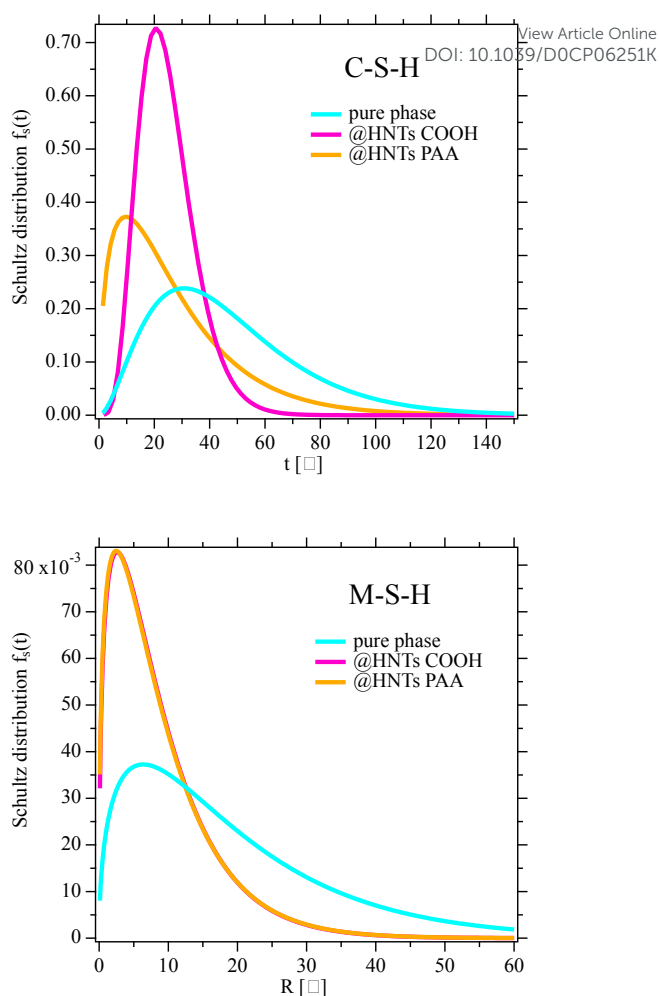


Fig. 5 Effective Schultz distribution of the total thickness $t = nL$ of the multilayer disk like globules in the C-S-H samples (top). Effective Schultz distribution of the radius R of the spherical globules in the M-S-H samples (bottom).

Table 2 Parameters extracted from the modelling of SAXS pattern by equation reported in the ESI file. Values in parentheses are standard deviations on the last significant figures. *Calcium silicate thickness L_2 is globally fitted as 3.47 Å according to the literature⁵.

C-S-H	R (Å)	L (Å)	L_2 (Å)	\bar{n}	R_e (Å)	ξ (Å)	Z_n	D
pure phase	145(9)	13.8(3)	3.47*	3.38(1)	90.2(9)	424(8)	1.9(1)	2.70(3)
HNT-COOH	66.3(7)	17.1(2)	3.47*	1.45(2)	43.4(7)	955(9)	5 (up)	2.55(2)
HNT-PAA	68.1(6)	14.0(3)	3.47*	1.94(1)	45.6(8)	676(7)	0.6(1)	2.59(1)
M-S-H	R (Å)					ξ (Å)	Z_R	D
pure phase	19.5(4)	-	-	-	-	116(1)	0.48(1)	2.94(2)
HNT-COOH	8.8(2)	-	-	-	-	344(4)	0.41(1)	2.94(3)
HNT-PAA	8.8(3)	-	-	-	-	350(5)	0.38(4)	2.95(1)

A similar effect has been already discussed for C-S-H formation in the presence of methylhydroxyethyl cellulose¹¹ and, in general, it is well known that the globular structure of C-S-H gel can be modified by different types of additives, especially the ones bearing a carboxylic moiety¹⁶.

The change in the globule size affects the fractal arrangement of the silicate phase as evidenced by the values of mass fractal dimension (D) and fractal cut-off (ξ) reported in Table 2. When added in C-S-H, nanoclays reduce the extension of the foil structure proper of the base unit giving a more porous matrix as evidenced by the slight decrease of the fractal dimension, D . Concurrently, the fractal cut-off (ξ) of the hydrate globules

ARTICLE

PCCP

increases of hundreds of nanometers as a result of the presence of the nanotubes that seem to connect larger fractal areas. Differently, M-S-H samples show the same fractal dimension D , even in the presence of the additives. This behaviour can be explained with the spherical nature of M-S-H globules, which decrease in size without changing the compactness of the aggregate. In addition, the presence of functionalised HNTs has a reduced effect on the M-S-H gel structure given the weaker interaction of the carboxylic moieties with Mg^{2+} ions. The main effect of the additives is a noticeable increase of ξ due to higher connectivity imposed by HNTs which play the role of bridging agent toward contiguous fractal domains.

Conclusions

The effect of polycarboxylic functionalised halloysite nanotubes on the microstructure of calcium and magnesium silicate hydrates was investigated in great detail. Nanoclays functionalised with carboxylic, HNT-COOH, or polycarboxylic groups, HNT-PAA, were successfully prepared and used for the synthesis of four composites: C-S-H@HNT-COOH, C-S-H@HNT-PAA, M-S-H@HNT-COOH, and M-S-H@HNT-PAA. The microstructure of the pure C-S-H and M-S-H and of the overmentioned composites was investigated by a multi-technique approach including small- and wide-angle X-ray scattering and scanning electron microscopy.

The results indicate that the morphology of the silicate hydrate phases in the composite samples at the micrometric level is not remarkably affected by the presence of the HNT-COOH additives. The halloysites, especially the one bearing the PAA moiety, are well distributed both on the surface and inside the silicate matrices as clearly observed from SEM micrographs, supporting a good compatibility of the silicates with the nanoclays. At the nanometric level, the co-presence of the contribution related to the different pure phases in the X-ray diffraction profiles reveals that halloysites do not change the atomic structure of the hydrates.

The results at an intermediate scale (1-300 nm), as obtained by SAXS, show that the presence of HNTs during silicate hydrates development in solution tends to decrease the size of the disk-like globules reducing the fractal packing of the hydrate globules, which therefore become more open in the range of a few hundred nanometers as indicated by the decrease of the mass fractal dimension. This effect is more evident in the case of C-S-H with respect to M-S-H probably due to the greater interaction of the carboxylic moiety with the Ca^{2+} ions.

The effect of HNTs on the microstructure of cement mortars was also assessed in other studies. In particular, it was proved that the introduction of nano-clays into cement composites can improve their mechanical properties⁷ and it was also showed that the long-term mechanical strength of the slag cement mortars was significantly improved by the presence of nanoclays. These results suggested that the activity of HNTs on the nucleation of calcium hydrosilicate (C-S-H) caused an enhancement of the mechanical strength of the final composite⁸.

This study highlights the effect of nanoclays on the structure of the main components of classical and “green” binders (C-S-H and M-S-H, respectively) at nano/meso scale. Further analysis of the effect of these additives on the hydration and the macroscopic properties of cement are necessary to correlate these parameters to the change in the microstructure observed in this work.

Conflicts of interest

The authors declare that they have no known competing financial interests or personal relationships that could have appeared to influence the work reported in this paper.

Acknowledgements

GF, LR, PB and EF partial financial support from Consorzio per lo sviluppo dei Sistemi a Grande Interfase (CSGI) and MIUR “Progetto Dipartimenti di Eccellenza 2018-2022” allocated to Department of Chemistry “Ugo Schiff”. SHC’s research cited and data utilized for this paper throughout the years were work at MIT supported by the DOE Office of Basic Energy Sciences (BES) under the Award No. DE-FG02-90ER45429 since 1990 to May 2017.

Authors thank Dr. Wei-Shan Chiang for kindly providing the fitting routines. Authors also wish to thank Dr. Peisi Le and Dr. Yi-Qi Yeh for the help during SAXS experiments and data reduction and Dr. F. Ridi for useful discussion.

References

- 1 E. M. Gartner and D. E. Macphee, A physico-chemical basis for novel cementitious binders, *Cement and Concrete Research*, 2011, **41**, 736–749.
- 2 E. Gartner and T. Sui, Alternative cement clinkers, *Cement and Concrete Research*, 2018, **114**, 27–39.
- 3 N. Vlasopoulos and C. R. Cheeseman, World Patent Application WO2009156740.
- 4 T. Zhang, C. R. Cheeseman and L. J. Vandeperre, Development of low pH cement systems forming magnesium silicate hydrate (MSH), *Cement and concrete research*, 2011, **41**, 439–442.
- 5 W.-S. Chiang, E. Fratini, P. Baglioni, D. Liu and S.-H. Chen, Microstructure determination of calcium-silicate-hydrate globules by small-angle neutron scattering, *The Journal of Physical Chemistry C*, 2012, **116**, 5055–5061.
- 6 J. Pourchez, B. Ruot, J. Debayle, E. Pourchez and P. Grosseau, Some aspects of cellulose ethers influence on water transport and porous structure of cement-based materials, *Cement and Concrete Research*, 2010, **40**, 242–252.
- 7 N. Farzadnia, A. A. Ali, R. Demirboga and M. P. Anwar, Effect of halloysite nanoclay on mechanical properties, thermal behavior and microstructure of cement mortars, *Cement and concrete research*, 2013, **48**, 97–104.
- 8 S. Allalou, R. Kheribet and A. Benmounah, Effects of calcined halloysite nano-clay on the mechanical properties and microstructure of low-clinker cement mortar, *Case Studies in Construction Materials*, 2019, **10**, e00213.

- 9 P. Hosseini, R. Hosseinpourpia, A. Pajum, M. M. Khodavirdi, H. Izadi and A. Vaezi, Effect of nano-particles and aminosilane interaction on the performances of cement-based composites: An experimental study, *Construction and Building Materials*, 2014, **66**, 113–124.
- 10 M. Tonelli, P. Baglioni and F. Ridi, Halloysite Nanotubes as Nano-Carriers of Corrosion Inhibitors in Cement Formulations, *Materials*, 2020, **13**, 3150.
- 11 W.-S. Chiang, G. Ferraro, E. Fratini, F. Ridi, Y.-Q. Yeh, U. S. Jeng, S.-H. Chen and P. Baglioni, Multiscale structure of calcium-and magnesium-silicate-hydrate gels, *Journal of Materials Chemistry A*, 2014, **2**, 12991–12998.
- 12 D. R. M. Brew and F. P. Glasser, Synthesis and characterisation of magnesium silicate hydrate gels, *Cement and Concrete Research*, 2005, **35**, 85–98.
- 13 Y. Joo, Y. Jeon, S. U. Lee, J. H. Sim, J. Ryu, S. Lee, H. Lee and D. Sohn, Aggregation and stabilization of carboxylic acid functionalised halloysite nanotubes (HNT-COOH), *The Journal of Physical Chemistry C*, 2012, **116**, 18230–18235.
- 14 H. Peng, R. Dong, S. Wang, Z. Zhang, M. Luo, C. Bai, Q. Zhao, J. Li, L. Chen and H. Xiong, A pH-responsive nano-carrier with mesoporous silica nanoparticles cores and poly (acrylic acid) shell-layers: fabrication, characterization and properties for controlled release of salidroside, *International journal of pharmaceutics*, 2013, **446**, 153–159.
- 15 U.-S. Jeng, C. H. Su, C.-J. Su, K.-F. Liao, W.-T. Chuang, Y.-H. Lai, J.-W. Chang, Y.-J. Chen, Y.-S. Huang and M.-T. Lee, A small/wide-angle X-ray scattering instrument for structural characterization of air–liquid interfaces, thin films and bulk specimens, *Journal of Applied Crystallography*, 2010, **43**, 110–121.
- 16 W.-S. Chiang, E. Fratini, F. Ridi, S.-H. Lim, Y.-Q. Yeh, P. Baglioni, S.-M. Choi, U.-S. Jeng and S.-H. Chen, Microstructural changes of globules in calcium–silicate–hydrate gels with and without additives determined by small-angle neutron and X-ray scattering, *Journal of colloid and interface science*, 2013, **398**, 67–73.
- 17 D. A. Almasri, N. B. Saleh, M. A. Atieh, G. McKay and S. Ahzi, Adsorption of phosphate on iron oxide doped halloysite nanotubes. *Sci. Rep.* 9, 3232, 2019.
- 18 D. Nied and A. Dauzères, Magnesium silicate hydrates (MSH): formation kinetics and range of composition, *Magnesium*, 2014, **14**, 17.
- 19 M. Tonelli, F. Martini, L. Calucci, E. Fratini, M. Geppi, F. Ridi, S. Borsacchi and P. Baglioni, Structural characterization of magnesium silicate hydrate: towards the design of eco-sustainable cements, *Dalton transactions*, 2016, **45**, 3294–3304.
- 20 Y. He, X. Zhao, L. Lu, L. J. Struble and S. Hu, Effect of C/S ratio on morphology and structure of hydrothermally synthesized calcium silicate hydrate, *Journal of Wuhan University of Technology-Mater. Sci. Ed.*, 2011, **26**, 770–773.
- 21 L. A. Feigin and D. I. Svergun, *Structure Analysis by Small-Angle X-Ray and Neutron Scattering*, Plenum Press, New York, 1987.

View Article Online
DOI: 10.1039/D0CP06251K